JOURNAL OF COMPUTATIONAL PHYSICS 117, 114–120 (1995)

Numerical Study of Barotropic and Baroclinic Behavior of a Nonlinear Two-Layer Model

STEFAN DIEBELS

Institut für Mechanik, Technische Hochschule Darmstadt, D-64289 Hochschulstraße 1, Darmstadt, Germany

Received January 4, 1993

The fluid motion in a strongly stratified lake can be described by a set of nonlinear dispersive partial differential equations derived from the equations of motion. These model equations are solved numerically by an implicit finite difference scheme. Variable topography and the influence of the free surface are taken into account as well as nonlinear and dispersive terms. The numerical solutions that are obtained are stable and in good agreement with experimental results. In the case of wind forcing, they show the typical transition from barotropic to baroclinic motion.

1. INTRODUCTION

The stratification of lakes during the summer months does not only give rise to the well-known surface waves. In addition to this external or barotropic motion internal, baroclinic modes are also possible [30, 18, 17] with generally more conspicuous signals. Usually, the vertical density profile is nearly constant in an upper and lower region of the lake while it is rapidly changing in a narrow band where the largest temperature gradient arises. This location is called thermocline. This density distribution is often modelled by two layers of different but constant densities separated by a discontinuity sheet at the location of the thermocline. Such two-layer models are able to predict the barotropic and the first baroclinic mode [17, 14]. Usually, the resulting equations are simplified by an explicit vertical integration over the thickness of the layers which leads to a reduction of the spatial dimensions. This procedure is well known in limnology and oceanography and allows the description of long waves travelling in shallow water [17, 8]. The resulting equations are either linear [13, 14, 3] and then allow further simplifications or else they are nonlinear and then of Boussinesq type [5, 6]. If only one direction of wave propagation is of interest the Korteweg–deVries equation can be recovered [21, 34, 10]. If wave propagation in fluids of finite or great depth is modelled, a vertical integration is still possible. That procedure then leads to so-called finite depth equations [15, 21] or to equations of the Benjamin–Davis–Ono type [4, 2].

When barotropic wave motion is not the focus it is a common procedure to eliminate from these equations the barotropic mode by using the rigid lid assumption because the interaction of both modes happens on a short time scale [34, 9] and the free surface signal is small compared to the elevation of the interface.

If the waves are excited by wind the barotropic mode is excited first; internal waves are generated afterwards. Therefore, the transient wind load is transformed into a system of eigenmodes of the model. Even if the surface disturbances are small the arising internal waves have large amplitudes and show a strong nonlinear behavior. For this reason it becomes necessary to model wind forcing by nonlinear equations.

The equations presented in the next section include nonlinear and dispersive terms as well as some frictional dissipation; they allow the excitation by wind forces and the decay processes by internal dissipation to be modelled [5, 6]. Because of the coupling of both possible modes and due to the nonlinearities, the equations generally defy an analytical solution, and one must resort to a numerical solution technique. In this paper an implicit numerical scheme is presented which solves the set of partial differential equations by a finite difference method. The proposed scheme leads to a stable solution of the equations and applications to particular situations agree well with the experimental results obtained by Schuster [32]. To our knowledge this computation is the first for which both possible modes of a nonlinear two layer model are calculated without elimination of the barotropic part.

The next section gives some details of the model equations used and explains the underlying physics. Then the numerical procedure is presented and some remarks on the stability are given. In the last section of the paper results obtained numerically are compared with experimental data and, as an additional application, wind forcing in a channel is modelled.

2. THE MODEL EQUATIONS

We shall confine our attention to the spatially one-dimensional case and therefore ignore effects of the rotation of the Earth. The more general two-dimensional case including Coriolis forces is treated by Diebels [5]. The following set of equations was derived by Diebels *et al.* [6]

$$(a_0 - a_1)_t + ((\alpha a_0 + h_1 - \alpha a_1)\bar{u}_1)_x = 0, \qquad (2.1)$$

0021-9991/95 $6.00

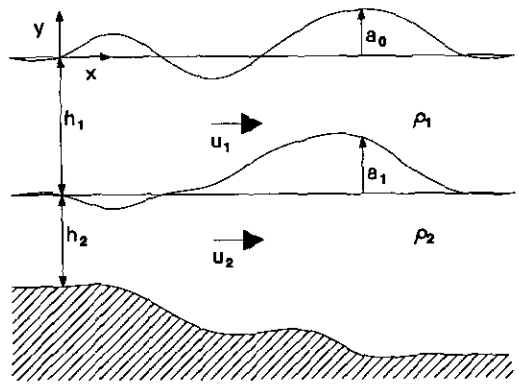

FIG. 1. Geometry and notation. The figure shows the surface $z = a_0(x, t)$, the interface between the layers $z = -h_1 + a_2(x, t)$ and the bottom $z = -(h_1 + h_2(x))$. The horizontal velocities u_1 and u_1 are marked as arrows.

$$a_{1t} + ((\alpha a_1 + h_2)\bar{u}_2)_x = 0, \tag{2.2}$$

$$\bar{u}_{1t} + \alpha\bar{u}_1\bar{u}_{1x} + a_{0x} - \varepsilon^2(\tfrac{1}{3}h_1^2\bar{u}_{1xxt} + \tfrac{1}{2}h_1(h_2\bar{u}_2)_{xxt}) = \tau_s - \tau_i, \tag{2.3}$$

$$\bar{u}_{2t} + \alpha\bar{u}_2\bar{u}_{2x} + \delta a_{0x} + (1 - \delta)a_{1x} - \varepsilon^2(\tfrac{1}{2}\delta h_1^2\bar{u}_{1xxt} + \tfrac{1}{2}h_2(h_2\bar{u}_2)_{xxt} - \tfrac{1}{6}h_2^2\bar{u}_{xxt}) = \tau_i - \tau_b. \tag{2.4}$$

Equations (2.1) and (2.2) result from a vertical integration of the continuity equation over the upper and the lower layers, respectively, and are known as kinematic wave equations. Here a_0 and a_1 are the elevations of the free surface and the interface, while $\bar{u}_1$ and $\bar{u}_2$ are the corresponding averaged horizontal velocities; see Fig. 1 for details. The parameter α is the ratio of a reference amplitude and a vertical length scale; α measures the influence of nonlinearity and is assumed to be small. The last equation pair (2.3) and (2.4) emerges from vertical integrations of the momentum equations where the pressure gradient was expressed by the horizontal gradient of the elevations. Taking into account the vertical acceleration leads to dispersive terms with third-order derivatives; these terms are weighted with the squared geometrical aspect ratio ε which equals the ratio of the vertical length scale to a typical wavelength. In general the aspect ratio ε is a small quantity in the shallow water theory. In deriving the equations it was assumed that nonlinearity and dispersion are connected by the Ursell number $\mathcal{U}$

$$\mathcal{U} = \frac{\alpha}{\varepsilon^2} = O(1). \tag{2.5}$$

This implies that effects due to nonlinearity and dispersion are of the same order and can balance; therefore, if friction is neglected, waves of permanent form should be possible [35, 11]. Frictional effects are modelled by the τ-terms on the right-hand side of the equations, which represent the stress tractions exerted at the surface (τ_s), at the interface (τ_i) and at the bottom (τ_b). It turned out that the following constitutive relations led to satisfactory reproduction of the attenuation of the waves:

$$\tau_s = \nu_s(u_{\text{wind}} - \bar{u}_1), \tag{2.6}$$

$$\tau_i = \nu_i(\bar{u}_1 - \bar{u}_2), \tag{2.7}$$

$$\tau_b = \nu_b\bar{u}_2, \tag{2.8}$$

in which the factors ν must be determined by experiments. Those performed by Schuster [32] show that the numerical values of the ν's depend on the chosen geometry; however, they are at least an order of magnitude smaller than the nonlinearity parameter α or the squared aspect ratio ε^2.

The quantity $\delta = \rho_1/\rho_2$ is the ratio of the density in the upper layer to that of the lower layer and is slightly smaller than unity, for which the fluid is stably stratified. We assume δ to be constant and unaffected by the motion; so thermocline erosion and any formation of local baroclinic instability is excluded.

The underlying physics of the above equations assumes long wave propagation. Nonlinearity and dispersion influence the motion, the observed amplitudes may be finite, and a finite aspect ratio is allowed. These limitations are fulfilled by many geophysical wave propagation phenomena. As limiting cases linear two-layer models are included [18, 17, 14, 30]. Also one-layer models can be recovered. If in the equations of the one-layer model the nonlinearity and dispersion are kept, then they are of Boussinesq type [28, 27, 37].

Diebels [5] has shown that the above set of equations leads to stable wave solutions in the linear limit; the resulting dispersion law coincides with that given by Lamb [16] if the latter is restricted to terms of second order in ε. The stability of the solution of the linear equations is, however, lost if a mathematical equivalent form of the nonlinear equations is used which transforms the third-order mixed derivatives into third-order spatial derivatives as known from the Korteweg–deVries equation.

In the next section we propose a finite difference scheme by which Eqs. (2.1)–(2.4) are solved without additional restrictions. The scheme reproduces the stability, which is exhibited by the linearized differential equations.

3. THE FINITE DIFFERENCE APPROXIMATION

3.1. *The Numerical Scheme*

Instead of the well-known predictor–corrector schemes often used in approximations of the shallow water equations of Boussinesq type [26, 25, 24] a single step implicit finite difference scheme is used to solve the linear part of the equations, i.e., all terms not involving a factor α in Eqs. (2.1)–(2.4). This scheme allows simultaneous prediction of both the barotropic

and baroclinic modes. The predictor–corrector schemes were not able to deal with both modes in one step for which reason additional restrictions became necessary, typically a rigid lid assumption was used to eliminate the barotropic mode [1, 20].

Spatial and temporal coordinates are discretized by the steps Δx and Δt, with $x = j\,\Delta x$ and $t = n\,\Delta t$, respectively. Each step is denoted by a subscript j for the jth space step and by a superscript n for the nth time step. Introducing the difference operators

$$\frac{\partial f}{\partial t} = \frac{f_j^{n+1} - f_j^n}{\Delta t} + O(\Delta t) = D_{tj}^n f + O(\Delta t), \tag{3.1}$$

$$\frac{\partial f}{\partial x} = \frac{f_{j+1}^{n+1} - f_{j-1}^{n+1}}{2\,\Delta x} + O(\Delta x^2) = D_{xj}^{n+1} + O(\Delta x^2) \tag{3.2}$$

leads to an implicit Eulerian differencing scheme for the leading linear terms.

The dispersive terms with mixed derivatives require also implicit differences. Using central differences for the second spatial derivative will not increase the band width of the resulting matrix. If we define the corresponding operator

$$D_{xxj}^n f = \frac{f_{j+1}^n - 2f_j^n + f_{j-1}^n}{\Delta x^2} + O(\Delta x^2) \tag{3.3}$$

the discretization of the dispersive terms reads

$$f_{xxt} = D_{tj}^n [D_{xxj}^n f] + O(\Delta x^2, \Delta t). \tag{3.4}$$

The simple choice of the dependence of the shear stresses on the velocity differences (2.6)–(2.8) allows a posteriori consideration of the forced motion or inclusion of dissipation without essentially increasing the numerical effort. Only a few coefficients of the marix in the emerging linear system must be altered.

By taking into account all these linear terms the set of equations which results from implicit differencing is represented by a band matrix with temporally constant coefficients that can be factorized once and for all. This advantage can be conserved if the weak nonlinearity is discretized in an explicit form, viz.,

$$(fg)_x = D_{xj}^n [fg] + O(\Delta x^2). \tag{3.5}$$

This choice happens to produce no instability problems of the scheme as long as the nonlinearity is weak. Hartig [12] uses a Newton algorithm in which he solves the nonlinearities also implicitly. His scheme, because of the iterations, has the disadvantage of consuming much more CPU time than our proposed scheme.

With the above operators the difference equations replacing the differential equations read

$$D_{tj}^n [a_0 - a_1] + D_{xj}^{n+1} [h_1 \bar{u}_1] + \alpha D_{xj}^n [(a_0 - a_1)\bar{u}_1] = 0, \tag{3.6}$$

$$D_{tj}^n a_1 + D_{xj}^{n+1} [h_2 \bar{u}_2] + \alpha D_{xj}^n [a_1 \bar{u}_2] = 0, \tag{3.7}$$

$$\begin{aligned} &D_{tj}^n [\bar{u}_1 - \tfrac{1}{3}\varepsilon^2 h_1^2 D_{xxj}^n \bar{u}_1 - \tfrac{1}{2}\varepsilon^2 h_1 D_{jxx}^n [h_2 \bar{u}_2]] \\ &+ \tfrac{1}{2}\alpha D_{xj}^n [\bar{u}_1^2] + D_{xj}^{n+1} a_0 + (\nu_s + \nu_i)\bar{u}_{1j}^{n+1} - \nu_i \bar{u}_{2j}^{n+1} = \nu_s u_{\text{wind}}, \end{aligned} \tag{3.8}$$

$$\begin{aligned} &D_{tj}^n [\bar{u}_2 - \tfrac{1}{2}\varepsilon^2\, \delta h_1^2 D_{xxj}^n \bar{u}_1 \\ &- \tfrac{1}{2}\varepsilon^2 h_2 D_{xxj}^n [h_2 \bar{u}_2] + \tfrac{1}{6}\varepsilon^2 h_2^2 D_{xxj}^n \bar{u}_2] \\ &+ \tfrac{1}{2}\alpha D_{xj}^n [\bar{u}_2^2] + D_{xj}^{n+1} [\delta a_0 + (1 - \delta) a_1] \\ &+ (\nu_i + \nu_b)\bar{u}_2^{n+1} - \nu_i \bar{u}_1^{n+1} = 0. \end{aligned} \tag{3.9}$$

They are valid for a channel in $0 < x < l$ corresponding to $0 < j < J$, respectively. This solution requires boundary conditions at the channel ends. If it is closed at $j = 0$ and $j = J$ with impermeable walls, the following boundary conditions apply for all time steps n

$$\bar{u}_{10}^n = 0, \quad \frac{a_{01}^n - a_{00}^n}{\Delta x} = O(\Delta x), \tag{3.10}$$

$$\bar{u}_{20}^n = 0, \quad \frac{a_{11}^n - a_{10}^n}{\Delta x} = O(\Delta x), \tag{3.11}$$

$$\bar{u}_{1J}^n = 0, \quad \frac{a_{0J}^n - a_{0(J-1)}^n}{\Delta x} = O(\Delta x), \tag{3.12}$$

$$\bar{u}_{2J}^n = 0, \quad \frac{a_{1J}^n - a_{1(J-1)}^n}{\Delta x} = O(\Delta x), \tag{3.13}$$

where the boundary conditions of Neumann type for the elevations are discretized by a forward and a backward difference, respectively, instead of central differences. This is the only place where the order of approximation is $O(\Delta x)$ rather than $O(\Delta x^2)$. Second-order approximation could be introduced for consistency, but is not important as the approximations (3.10)–(3.13) are localized.

3.2. *Stability*

The stability of the proposed scheme is examined in the usual way by using Fourier analysis [31, 19]. This method is only applicable to linear equations with constant coefficients. Therefore, the nonlinear terms are neglected in this analysis, $\alpha = 0$. Further restrictions arise because the coefficients must be constant. The stability criterion cannot be established for variable topography, and so we set h_2 constant here. Furthermore, external forcing and boundary conditions cannot be handled by this method. Computations, however, showed that the stability exhibited by the simplified equations carries over to the general set of equations provided the physical restrictions of the model are fulfilled.

If h_2 is constant the dispersive terms can be collected in Eqs. (2.3) and (2.4) by using the abbreviations

$$\beta_1 = \tfrac{1}{3}h_1^2, \tag{3.14}$$

$$\beta_2 = \tfrac{1}{2}h_1h_2, \tag{3.15}$$

$$\gamma_1 = \tfrac{1}{2}\,\delta h_1^2, \tag{3.16}$$

$$\gamma_2 = \delta h_1h_2 + \tfrac{1}{3}h_2^2. \tag{3.17}$$

They then become

$$-\varepsilon^2(\beta_1\bar{u}_1 + \beta_2\bar{u}_2)_{xxt}, \tag{3.18}$$

$$-\varepsilon^2(\gamma_1\bar{u}_1 + \gamma_2\bar{u}_2)_{xxt} \tag{3.19}$$

in the momentum equation of the upper and of the lower layers, respectively.

To examine the stability of the linearized field equations the spatial variation of each quantity is replaced by a Fourier transform

$$f_j^n \to \hat{f}(k)\exp \mathrm{i}kj\,\Delta x \tag{3.20}$$

with an arbitrary wave number k. In doing so the first and second spatial derivatives can be expressed as

$$D_{xj}^n f \to \quad \mathrm{i}\hat{f}^n(k)\frac{\sin k\,\Delta x}{\Delta x} \quad =: \frac{\mathrm{i}\hat{f}^nS}{\Delta x}, \tag{3.21}$$

$$D_{xxj}^n f \to 2\hat{f}^n(k)\frac{\cos(k\,\Delta x) - 1}{\Delta x^2} =: \frac{2\hat{f}^nC}{\Delta x^2}. \tag{3.22}$$

Collecting the amplitudes $\hat{a}_0(k, t)$, $\hat{a}_1(k, t)$, $\hat{u}_1(k, t)$, and $\hat{u}_2(k, t)$ for the elevations and mean velocities as a four vector and employing matrix notation, the transformed equations take the form

$$\mathbf{A}\mathbf{x}^{n+1} = \mathbf{B}\mathbf{x}^n, \tag{3.23}$$

where

$$\mathbf{x}^n = (\hat{a}_0^n, \hat{a}_1^n, \hat{u}_1^n, \hat{u}_2^n)^{\mathrm{T}} \tag{3.24}$$

and

$$\mathbf{A} = \begin{pmatrix} 1 & -1 & \mathrm{i}\dfrac{\Delta t}{\Delta x}h_1S & 0 \\ 0 & 1 & 0 & \mathrm{i}\dfrac{\Delta t}{\Delta x}h_2S \\ \mathrm{i}\dfrac{\Delta t}{\Delta x}S & 0 & 1 - \dfrac{2\varepsilon^2\beta_1}{\Delta x^2}C + \nu_s + \nu_i & -\dfrac{2\varepsilon^2\beta_2}{\Delta x^2}C - \nu_i \\ \mathrm{i}\,\delta\dfrac{\Delta t}{\Delta x}S & \mathrm{i}(1-\delta)\dfrac{\Delta t}{\Delta x}S & -\dfrac{2\varepsilon^2\gamma_1}{\Delta x^2}C - \nu_i & 1 - \dfrac{2\varepsilon\gamma_2}{\Delta x^2}C + \nu_i + \nu_b \end{pmatrix}, \tag{3.25}$$

$$\mathbf{B} = \begin{pmatrix} 1 & 0 & 0 & 0 \\ 0 & 1 & 0 & 0 \\ 0 & 0 & 1 - \dfrac{2\varepsilon^2\beta_1}{\Delta x^2}C & -\dfrac{2\varepsilon^2\beta_2}{\Delta x^2}C \\ 0 & 0 & -\dfrac{2\varepsilon^2\gamma_1}{\Delta x^2}C & 1 - \dfrac{2\varepsilon\gamma_2}{\Delta x^2}C \end{pmatrix}. \tag{3.26}$$

The standard stability criterion is defined for a matrix equation in the form [29, 31]

$$\mathbf{x}^{n+1} = \mathbf{A}^{-1}\mathbf{B}x^n. \tag{3.27}$$

Then the stability depends on the norm of the eigenvalues of the matrix $\mathbf{A}^{-1}\mathbf{B}$: If the moduli of all eigenvalues are less than unity no component is magnified by the time step.

The eigenvalue problem $\mathbf{A}^{-1}\mathbf{B} - \lambda\mathbf{I}$ was treated numerically. For chosen geometry h_1 and h_2 and $dt = dx$ the matrix $\mathbf{A}$ was evaluated, inverted, and then the matrix product was computed. Using a standard algorithm for the eigenvalue problem [7] all examined geometrical configurations led to eigenvalues λ with their moduli equal or less than unity even in cases where the viscosities ν_s, ν_i, and ν_b were all set to zero. Eigenvalues of modulus one were simple. This stable behavior is well known from implicit finite difference schemes.

Beyond this linear analysis experimenting with the nonlinear equations including variable topography indicated stability for the choice $dt = dx$, provided that the physical limitations of the model were observed.

Figure 2 shows the dependence of the maximum amplitude on the step size Δx for fixed initial and geometrical conditions. If fewer than 400 grid points were used (corresponding to $\Delta x = 0.025$), a strong dependence of the maximum amplitude and of the wave form on Δx is found. However, for more than

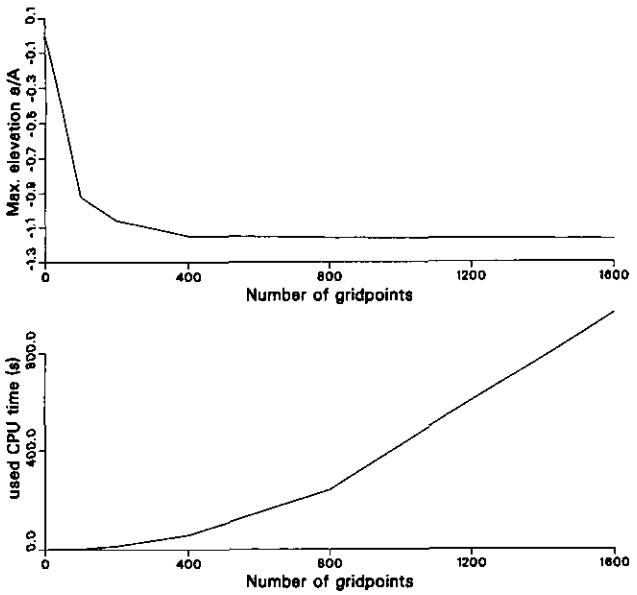

FIG. 2. Influence of the step size. The upper part of the figure shows the dependence of the maximum amplitude on the number of grid points. If more than 400 grid points are used the influence is less than 10%. The lower part of the figure shows the dependence of the charged CPU time on the number of grid points. It is increasing rapidly when the number of grid points is increased. Figure 3 shows the corresponding time series.

400 grid points the amplitude becomes nearly independent of the number of grid points while the consumed CPU time increased rapidly. The choice of 400 grid points was regarded as an acceptable compromise for the problem especially when the shape of the computed waves had to be predicted. Figure 3 shows the calculated time series for 100 (Δx = 0.1), 200 (Δx = 0.05), 400 (Δx = 0.025), 800 (Δx = 0.0125), and 1600 (Δx = 0.00625) grid points. The shape of the waves does not depend on the step size if 400 and more grid points are used. Therefore the following applications were all calculated with 400 grid points for the spatial discretization. The dimensionless quantities are chosen to be the same as those for the calculations presented in Figs. 2 and 3.

4. APPLICATIONS

4.1. *Comparison with Experiments*

Schuster [32] built an experimental device which allowed observations of nonlinear wave propagation in a two layer fluid, Fig. 4. A 10-m long channel of 33 × 33 cm^2 cross section was filled with fresh and salt water of different layer depths. Stratification was such that δ = 0.98. At the left end of the channel a wave generator was installed which excites the internal mode by moving the same volume of fluid in both layers in opposite directions. At six positions, P1 to P6, the time series of the elevations of the interface were recorded by conductivity measurements. In Fig. 5 the measured time series at positions P1 to P6 are compared with those obtained from numerical computations. A detailed description of how the experiments were performed and this comparison is achieved is reserved for a different paper; see Schuster *et al.* [33]. The displayed data reproduce the propagation of an internal soliton-like wave over a shelf which is positioned at gauge P3 and blocks 70% of the lower layer. The observed wave behaves like a soliton for a short time, but due to friction the amplitude decreases and the wave is no longer a wave of permanent form; therefore we call it a soliton-like wave. It travels from the left end of the channel with nearly constant speed until it reaches the shelf. Then the wave splits into an oscillating wave train which is transmitted over the shelf while a very small part of the incoming wave is reflected. On the shelf, because of a reduction of equivalent depth, the phase speed is smaller than it is in the deep region. Behind the shelf the wave transforms again into a solitary type wave and stabilizes as such. Later, the wave is completely reflected at the right end of the channel and travels back to the left.

In Fig. 5 the solid lines reproduce the measured data of Schuster [32] while the dashed lines represent the calculated time series using the above described numerical scheme. As can be seen the agreement between numerical results and experimental data is excellent. The model achieves reproduction of the whole evolution of the wave, starting from the generation at the left end of the channel over the fission of the transmitted and reflected wave at the shelf to the reflection at the right end

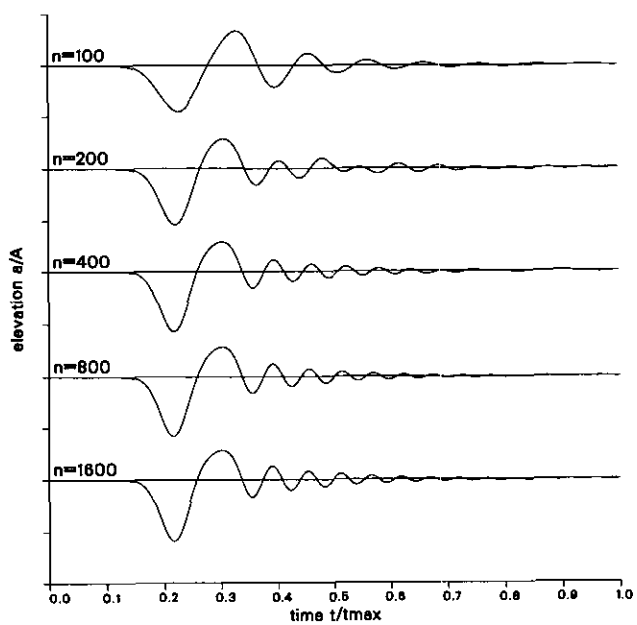

FIG. 3. Waveform depending on the step size. Time series for 100, 200, 400, 800, and 1600 grid points are shown. The calculated time intervals are the same for all five computations. Increasing the number of grid points leads to a slight increase of the phase speed and to a steepening of the leading wave. A dependence of the wave form for more than 400 grid points cannot be discerned.

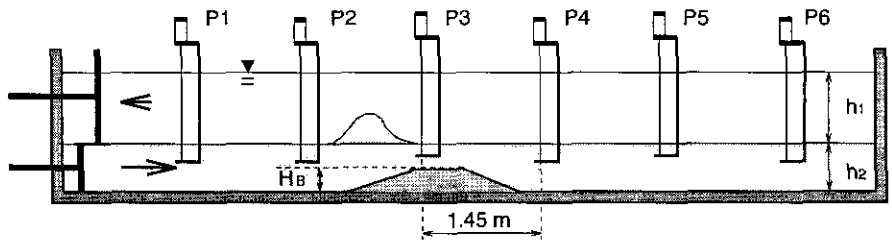

FIG. 4. Experimental setup. Channel with gauges and shelf.

of the channel. Previous comparisons of experimental data and the sech^2-soliton solution of the Korteweg–deVries equation [23, 22, 34] led to an agreement of the shape of the wave; however, a comparison of the complete evolution of internal waves was not achieved.

4.2. *Wind Forcing*

Wind forcing is the main energy input into lakes and leads to large internal waves if a stratification is present. These processes can also be modeled with our numerical scheme, when a wind force is introduced as a shear stress acting on the free surface. Our model computations start from a state of rest; a constant shear stress is applied uniformly at the free surface at time $t = 0$, maintained for a time, which is small in comparison to the time, which a baroclinic wave needs to travel in the channel and then suddenly is switched off. Figure 6 shows the calculated time series of the surface elevation and of the internal elevation at the gauges P1 and P6. To visualize the surface elevation it was magnified by a factor of 50. The barotropic mode is immediately excited while it takes some time before the interface starts moving. While the wind blows from left to right the interface is depressed at the right end of the channel, whereas it rises at the left end. This is well known for up- and down-welling processes. A large internal depression wave moves from the right to the left and a large internal wave of elevation travels in opposite direction. These waves decay into oscillating wave trains. The internal motion leads to a modulation of the free surface which can also be discerned in Fig. 6. This surface signal is the trace allowing the detection of large internal waves in the ocean [23, 22, 36].

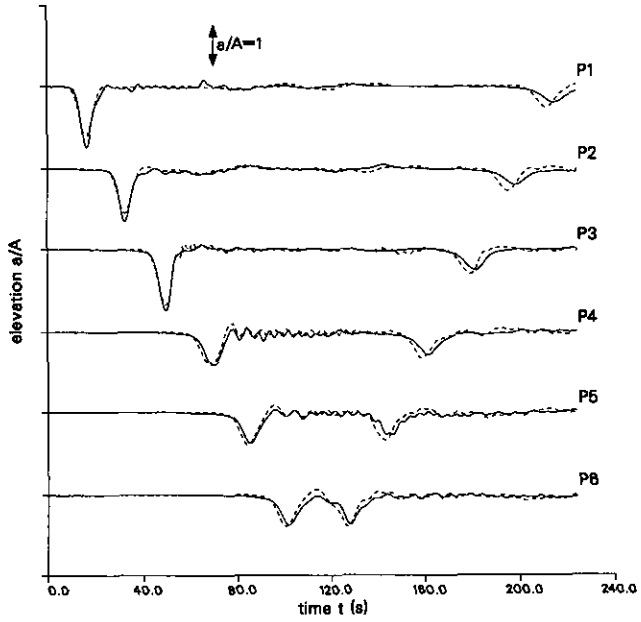

FIG. 5. Comparison of experimental data and computations. Wave propagation over variable topography. Solid lines represent time series of experimental data; dashed lines stand for computational results. The geometry of the shelf and the positions of the gauges are shown in the previous Fig. 4. The shelf blocks 70% of the lower layer.

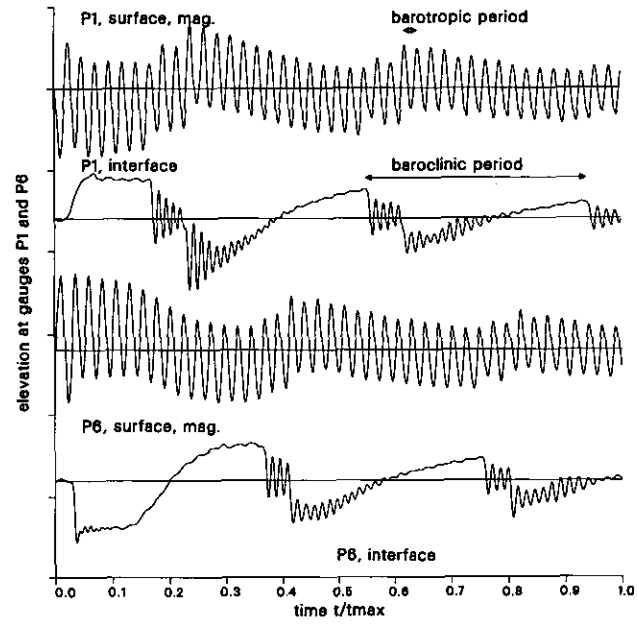

FIG. 6. Model response to wind forcing. Comparison of the surface elevation (magnified by a factor of 50) and the internal elevation recorded at the left and right ends of the channel after a short wind input. Both eigenmodes are excited.

5. CONCLUSIONS

The purpose of this paper was the presentation of a nonlinear equation set for the propagation of barotropic and baroclinic waves in a two-layered fluid system and its numerical solution by an implicit and stable finite difference technique. The proposed scheme was shown to be unconditionally stable for the linearly reduced equations with constant coefficients; its application to the complete nonlinear equations was shown to exhibit stable behavior, provided the model equations, initial and boundary conditions conform with the limiting physical assumptions, for which the model equations were derived. Both, forced and free weakly nonlinear waves in a nonrotating channel can be computed with their aid.

One special feature of the equations and their successful finite difference approximation is the simultaneous determination of the motions of the free surface and the interface between the layers; i.e., no rigid-lid assumption had to be invoked. Another speciality is that variable topography is incorporated. Furthermore, dissipation can easily be worked into the equations without changing the main part of the integration routines.

These properties are essential in spatially two-dimensional applications of propagation of internal waves in the ocean and in lakes where also effects of the rotation of the Earth must be incorporated. These equations have been derived [5], and we are optimistic that their numerical treatment along these lines will be successful. Such a model can then be used in ocean wave problems in shelf regions or in lakes.

ACKNOWLEDGMENTS

This work derives in parts from [5] and results from the project *Interne Wellen in Seen-Experimentelle und theoretische Analyse.* It was financially supported by the Deutsche Forschungsgemeinschaft. I thank B. Schuster for his permission to use the experimental data and K. Hutter and G. Lill for many fruitful discussions concerning the numerical scheme and its stability.

REFERENCES

1. P. Beckers, These No. 819, Ecole Polytechnique federale de Lausanne, 1989 (unpublished).
2. T. J. Benjamin, *J. Fluid Mech.* **29,** 559 (1967).
3. J. G. Charney, *J. Mar. Res.* **14,** 477 (1955).
4. R. E. Davis and A. Acrivos, *J. Fluid Mech.* **29,** 593 (1967).
5. S. Diebels, *Interne Wellen—Ein Modell, das Nichtlinearität, Dispersion, Corioliseffekte und variable Topographie enthält,* Dissertation, Technische Hochschule Darmstadt, 1992.
6. S. Diebels, B. Schuster, and K. Hutter, to appear.
7. G. Engeln-Müllges and F. Reuter, *Formelsammlung zur numerischen Mathematik mit C-Programmen* (BI Wissenschaftsverlag, 1990).
8. A. E. Gill, *Atmosphere–Ocean Dynamics,* International Geophysics Series, Vol. 30 (Academic Press, New York/London, 1982).
9. R. H. J. Grimshaw, "Solitary Waves in Density Stratified Fluids," *Nonlinear Deformation Waves,* edited by U. Nigul and J. Engelbrecht (Springer-Verlag, New York/Berlin, 1983), p. 431.
10. R. H. J. Grimshaw, "Theory of Solitary Waves in Shallow Fluids," *Encyclopedia of Fluid Mechanics,* edited by N. P. Cheremisinoff (Gulf, Houston, 1986), p. 3.
11. J. L.Hammack and H. Segur, *J. Fluid Mech.* **84,** (1978).
12. M. Hartig, Diplomarbeit, Fachbereich Mathematik, Technische Hochschule Darmstadt, 1992 (unpublished).
13. K. Hutter, "Fundamental Equations and Approximations," *Hydrodynamic Modelling of Lakes,* edited by K. Hutter (Springer-Verlag, New York/Berlin, 1984), p. 1.
14. K. Hutter, "Linear Gravity Waves, Kelvin and Poincaré Waves, Theoretical Modelling and Observations," *Hydrodynamic Modelling of Lakes,* edited by K. Hutter (Springer-Verlag, New York/Berlin, 1984), p. 39.
15. T. Kubota, D. R. S. Ko, and L. D. Dobbs, *J. Hydronautics* **12,** 157 (1978).
16. H. Lamb, *Hydrodynamics* (Cambridge Univ. Press, London, 1932).
17. P. H. LeBlond and L. A. Mysak, *Waves in the Ocean,* Oceanography Series, (Elsevier, Amsterdam, 1978).
18. J. Lighthill, *Waves in Fluids* (Cambridge Univ. Press, Cambridge, 1978).
19. A. R. Mitchell, *Computational Methods in Partial Differential Equations* (Wiley, New York, 1977).
20. G. Mørk, B. Gjevik, and S. Holte, "Long Internal Waves in Lakes," *Second international Symposium on stratified flows,* edited by T. Carstens and T. McClimas (Tapir, Troudheim, 1980), p. 988.
21. L. A. Mysak, "Nonlinear Internal Waves," *Hydrodynamic Modelling of Lakes,* edited by K. Hutter (Springer-Verlag, New York/Berlin, 1984), p. 129.
22. A. R. Osborne, "The Generation and Propagation of Internal Solitons in the Andaman Sea," *Soliton Theory: A Survey of Results,* edited by A. P. Fordy (Manchester Univ. Press, Manchester, UK, 1990), p. 152.
23. A. R. Osborne and T. L. Burch, *Science* **208,** 451 (1980).
24. G. Pedersen, Preprint Series, Vol. 1, Institue of Mathematics, University of Oslo, 1989 (unpublished).
25. G. Pedersen and O. B. Rygg, Research Report in Mechanics, University of Oslo, Deparement of Mathematics, 1987 (unpublished).
26. D. H. Peregrine, *J. Fluid Mech.* **25,** 21 (1966).
27. D. H. Peregrine, *J. Fluid Mech.* **27,** 815 (1967).
28. D. H. Peregrine, "Equation for Water Waves and the Approximation behind Them," *Waves on Beaches and Resulting Sediment Transport,* edited by R. E. Meyer (Academic Press, New York/London, 1972), p. 95.
29. R. Peyret and T. D. Taylor, *Computational Methods in Fluid Flow* (Springer-Verlag, New York/Berlin, 1982).
30. O. M. Phillips, *The Dynamics of the Upper Ocean* (Cambridge Univ. Press, Cambridge, 1977).
31. W. H. Press, B. P. Flannery, S. A. Teukolsky, and W. T. Vetterling, *Numerical Recipes* (Cambridge Univ. Press, Cambridge, 1986).
32. B. Schuster, *Experimentelle Studie zur luteraktion nicht linearer, interner Wellen mit variablen Boden topographien in einem Rechteckkaual,* Dissertation, Technische Hochschule Darmstadt, 1992.
33. B. Schuster, S. Diebels, and K. Hutter, in preparation.
34. H. Segur and J. L. Hammack, *J. Fluid Mech.* **118,** 285 (1982).
35. F. Ursell, *Proc. Cambridge Philos. Soc.* **49,** 685 (1953).
36. P. D. Weidman, B. Dagyani, and G. Born, in *Wave Phenomena II: Modern Theory and Applications, Thirteenth Annual Conference of the Canadian Applied Mathematics Society, 1992* (unpublished).
37. T. Y. Wu, *J. Eng. Mech. Div. Proc. Am. Soc. Civil Eng.* **107,** 501 (1981).